Baltic Astronomy, vol. 15, 211–218, 2006.

ON THE EMPIRICAL INSTABILITY DOMAINS FOR PULSATING SUBDWARF B STARS

G. Fontaine[1], E. M. Green[2], P. Chayer[3], P. Brassard[1], S. Charpinet[4] and S. K. Randall[1]

[1] *Département de Physique, Université de Montréal, C.P. 6128, Succ. Centre-Ville, Montréal, Québec H3C 3J7, Canada*

[2] *Steward Observatory, University of Arizona, Tucson, AZ 85721, U.S.A.*

[3] *Bloomberg Center for Physics and Astronomy, The Johns Hopkins University, Baltimore, MD 21218-2686, U.S.A.*

[4] *Observatoire Midi-Pyrénées, 14 Av. E. Belin, F-31400 Toulouse, France*

Received 2005 August 1

Abstract. We present some of the results of an ongoing spectroscopic survey to derive reliable atmospheric parameters for the known pulsating sdB stars as well as several known constant stars. This survey involves high S/N ratio optical observations in conjunction with detailed NLTE model atmospheres. The homogeneity of our approach allows us, for the first time, to discuss with some confidence the locations of the empirical instability regions for the short-period pulsating EC 14026 stars and for the long-period PG 1716 stars in the surface gravity-effective temperature plane. We also briefly address the question of the influence of a weak stellar wind on these pulsators.

Key words: stars: hot subdwarfs – stars: oscillations

1. INTRODUCTION

It is now well established that stellar pulsations are a common phenomenon among hot B subdwarf (sdB) stars. A first type of pulsating sdB stars, called EC 14026 stars after the prototype EC 14026−2647, was discovered some years ago (Kilkenny et al. 1997), while the existence of a second type, the PG 1716 stars (after the prototype PG 1716+426), was reported only recently (Green et al. 2003). The relatively short pulsation periods observed in the EC 14026 stars – typically in the range 100–200 s – are attributed to p-mode oscillations, while the much longer periods detected in the PG 1716 stars – from 3000 s to upward of 8000 s – are attributed to g-mode pulsations (see, e.g., Fontaine et al. 2003).

In order to fully understand the properties of the pulsating sdB stars, it is necessary to have, among other things, a reliable description of the instability regions in the log g vs. $T_{\rm eff}$ diagram. The most recent discussion of the empirical instability strips for pulsating sdB stars was presented by Fontaine et al. (2004). However, that discussion remained limited because the estimates of the atmospheric parameters for pulsating sdB stars available at the time came from various mixed sources, potentially sporting significant systematic differences. As a consequence, only a somewhat blurred view of the empirical instability regions in the log g vs. $T_{\rm eff}$ plane could be provided.

Since then, we have worked hard to improve the situation by pursuing a spectroscopic program which emphasizes high S/N ratio observations and homogeneity of approach. We have now determined the atmospheric parameters of almost all known pulsating sdB stars accessible from Arizona, as well as many known constant stars for comparison purposes. We report here on the preliminary results of that ongoing program.

2. AN HOMOGENEOUS APPROACH THROUGH SPECTROSCOPY

Our approach has been part of a global optical spectroscopy program designed to improve on the characterizing of sdB stars. So far, we have gathered medium resolution (~ 1 Å), high signal-to-noise ratio ($< S/N > \sim 170$) spectra for 115 stars with the blue spectrograph at the new 6.5 m Multiple Mirror Telescope (MMT). Those spectra cover the range from ~ 4000 Å to ~ 4950 Å. Most of these stars have been searched by one of us (E.M.G.) for long-period photometric activity of the PG 1716 type. Several have also been searched by Billères et al. (2002) for short-period pulsations and found to be constant. In addition, we also gathered low resolution (~ 9 Å) spectra of even higher sensitivity ($< S/N > \sim 273$) for a sample of 55 stars at the Steward Observatory 2.3 m telescope. Those latter spectra cover the range from ~ 3615 Å to ~ 6900 Å and all belong to pulsating sdB's, either of the EC 14026 type or PG 1716 category. A detailed comparison of the 38 objects in common in the two samples has allowed us to conclude that, in spite of different resolution and spectral coverage, there are no significant systematic differences in the inferred atmospheric parameters of stars belonging to either one of the two samples. We explain that in terms of sufficiently high S/N ratio.

An integral part of our program is the development of a bank of model atmospheres and synthetic spectra suitable for the analysis of the spectroscopic data. To this end, we have so far computed two detailed grids (one in LTE and the other in NLTE) with the help of the public codes TLUSTY and SYNSPEC (Hubeny & Lanz 1995; Lanz & Hubeny 1995). Each grid is defined in terms of 11 values of the effective temperature (from 20 000 K to 40 000 K in steps of 2000 K), 10 values of the surface gravity (from log g of 4.6 to 6.4, in steps of 0.2 dex) and 9 values of the helium-to-hydrogen number ratio (from log $N(\mathrm{He})/N(\mathrm{H})$ of -4.0 to 0.0, in steps of 0.5 dex). These grids were originally developed to analyze our MMT data and, therefore, our current synthetic spectra are limited to the range from 3500 Å to 5800 Å, but this can easily be widened as needed. We are planning to include metals in the near future. More details about these models will be found in Green, Fontaine & Chayer (in preparation).

We show in Figure 1 the results of our analysis for our current sample of 115 sdB stars with MMT spectroscopy. Those were obtained with the help of our NLTE grid of He/H models. The figure illustrates the three atmospheric parameters that were inferred: log g, $T_{\rm eff}$ and the He/H number ratio. The size of each point is proportional to the logarithm of that latter quantity. In comparison to the normal (solar) He/H ratio (illustrated here by the open circle), all of the stars observed show helium deficiencies in their atmospheres. The observed pattern of He/H ratios is, however, rather complicated and defies simple explanations.

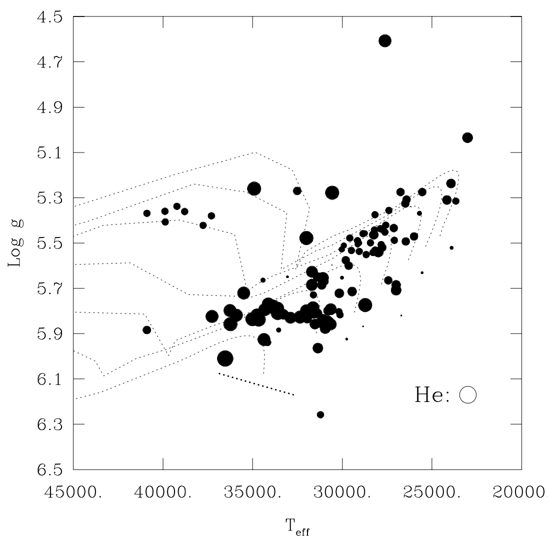

Fig. 1. Distribution of 115 sdB stars with MMT spectroscopy in the log g vs. $T_{\rm eff}$ diagram. The size of a circle gives a logarithmic measure of the inferred He/H number ratio. The thin dotted lines show some of Ben Dorman's evolutionary tracks for models with a range of H envelope masses. The thick dotted line represents the zero-age He-burning main sequence for masses with 0.3−0.6 $M_{\odot}$.

3. AN UPDATED VIEW OF THE EMPIRICAL INSTABILITY REGIONS

Figure 2 shows our updated view of the locations of the instability domains for pulsating sdB stars in the log g vs. $T_{\rm eff}$ plane as calculated from our He/H NLTE model atmospheres. It is possible, even probable, that the inclusion of metals will modify the picture somewhat. We are planning to investigate that point in the near future with the computations of NLTE models that would include metals along with H and He. For the time being, however, this is what we can offer. The built-in homogeneity of our approach is of central interest here; we show only stars for which we obtained spectra ourselves with the same instruments and that were analyzed in the same way.

All of the 30 known PG 1716 pulsators (except for one whose recent discovery was announced by Kilkenny et al. 2006) are plotted in Figure 2 and are shown as open circles. It can be seen that a typical PG 1716 star has a log g value of about 5.4 and an effective temperature of about 27 000 K. As indicated above, PG 1716 stars are long-period, high-order g-mode pulsators. In comparison, there are 34 known short-period, low-order p-mode pulsators of the EC 14026 type. The positions of 26 of these objects belonging to our homogeneous spectroscopic sample are plotted as filled circles in the figure. It is apparent that a typical EC 14026 star has a log g value of around 5.7 and an effective temperature of about 33 000 K, but there is some dispersion as well.

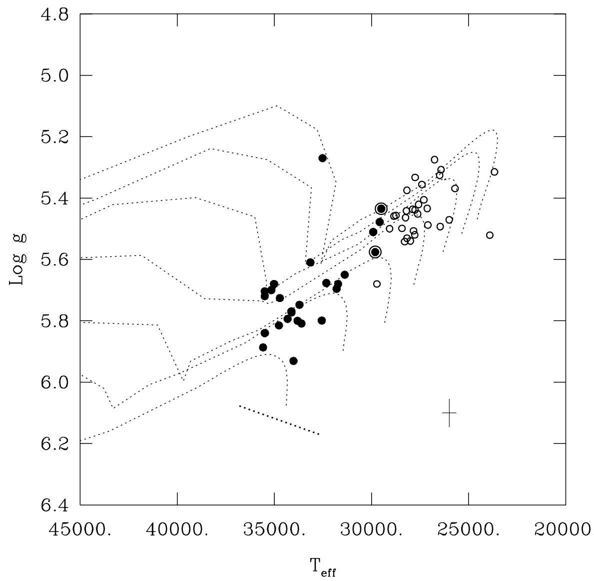

Fig. 2. Distribution of the pulsating sdB stars in the log g vs. $T_{\rm eff}$ diagram. The filled circles give the locations of 26 EC 14026 stars, while the open circles indicate those of 30 PG 1716 pulsators. The cross indicates typical uncertainties on the atmospheric parameters, while the curves are the same as in Fig. 1.

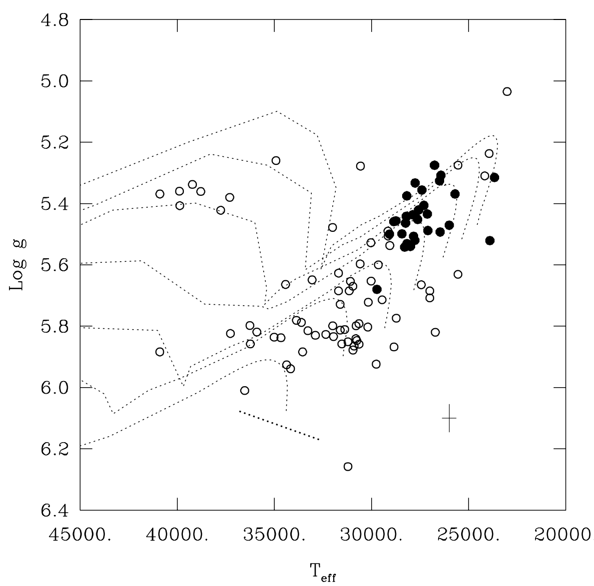

Fig. 3. Distribution of the sdB stars in the log g vs. $T_{\rm eff}$ diagram which have been searched for long-period photometric variations of the PG 1716 type. The filled circles give the locations of the 30 known PG 1716 pulsators, while the open circles indicate those of 70 constant stars. The other features in the figure are the same as in Fig. 2.

Figure 2 clearly shows that the two classes of pulsating sdB stars occupy different domains in the log g vs. $T_{\rm eff}$ plane, although the domains actually touch. As a matter of fact, two stars initially discovered as short-period pulsators have been reported to also exhibit long-period luminosity variations more characteristic of PG 1716 stars. These are HS 0702+6043 (Schuh et al. 2005) identified in the figure by the upper filled circle surrounded by a larger open circle and Balloon 090100001 (Oreiro et al. 2005; Baran et al. 2005) identified by the lower similar symbol. The positions of these two objects at the common boundary of the two classes of pulsating sdB stars are quite consistent with the suggestion that HS 0702+6043 and Balloon 090100001 are both EC 14026 and PG 1716 pulsators at the same time!

We show, in Figure 3, the distribution of the sdB stars which have been searched for long-period photometric activity of the PG 1716 type. The plot includes the locations of 30 (out of 31) known long-period pulsators (filled circles) and the locations of 70 constant stars (open circles). The latter are defined as stars with amplitude limits of less than $\sim$1 mmag in the period range 400$-$15 000 s (E.M.G., unpublished). We note that all of the objects illustrated in the figure belong to our MMT sample, hence the figure does provide an homogeneous view of the PG 1716 phenomenon in the log g vs. $T_{\rm eff}$ plane.

We also cannot help but point out the strong concentration of PG 1716 stars on the low-gravity cool side of the sdB range. Actually, at least two of the four apparently constant stars in that region may show very low-amplitude variations, but we prefer to adopt a conservative selection criterion and declare them "constant" for the time being. More generally, we cannot exclude the possibility that *all* cool sdB stars of low gravity may be PG 1716 pulsators at this stage.

The corresponding homogeneous view of the EC 14026 phenomenon is shown in Figure 4. In that figure, we plotted the positions of the 26 EC 14026 stars (out of 34 currently known) and of the 33 constant stars for which we have spectroscopic measurements. The latter are defined as stars with amplitude limits of less than $\sim$1 mmag in the period range 20$-$1 000 s (see Billères et al. 2002). As discussed by Charpinet et al. (2006), it is a remarkable fact that *all* of the known pulsators are found in the region of maximum p-mode instability as obtained through detailed nonadiabatic calculations using equilibrium models that include radiative levitation of iron. We take this as a strong observational proof of the basic validity of the driving mechanism based on radiative levitation as originally proposed by Charpinet et al. (1997) for EC 14026 stars.

At the same time, the possibility that variable and nonvariable stars may coexist in the EC 14026 instability domain was first hinted at by Billères et al. (1997) on the basis of early statistics. The homogeneous spectroscopy presented here confirms that this is indeed the case. Fig. 4 clearly reveals that sdB stars show a mixed population of variable and nonvariable stars inside the EC 14026 instability strip. The best contending mechanism to explain this phenomenon is the possibility that weak stellar winds significantly perturb the levitating reservoir of iron or iron-peak elements in some cases (see, e.g., Charpinet, Fontaine & Brassard 2001). We briefly discuss this possibility in the rest of this paper.

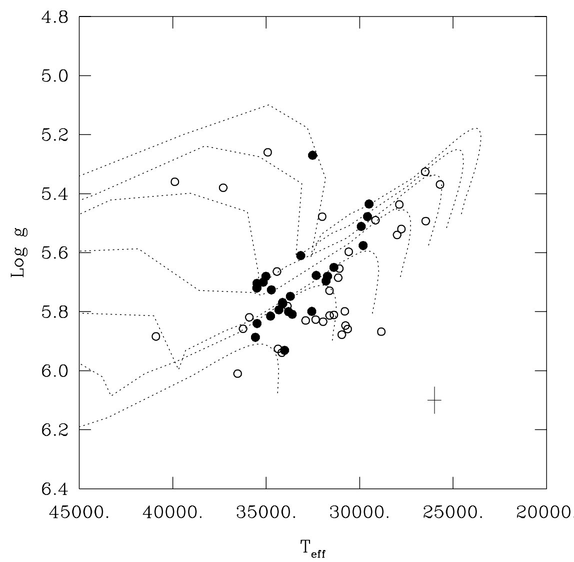

Fig. 4. Distribution of the sdB stars in the log g vs. $T_{\rm eff}$ diagram which have been searched for short-period photometric variations of the EC 14026 type, and which belong to our homogeneous spectroscopic sample. The filled circles give the locations of 26 EC 14026 pulsators, while the open circles indicate those of 33 constant stars. The other features in the figure are the same as in Fig. 2.

4. EFFECTS OF A STELLAR WIND ON THE SDB PULSATORS

The effects of a weak stellar wind on the levitating reservoir of iron in a typical model of a sdB star have already been discussed by Chayer et al. (2004). We have followed up on these calculations by integrating them into our equilibrium model building code and then analyzing the pulsational properties of such an evolving model with the help of our nonadiabatic pulsation code. We recall that the model considered by Chayer et al. (2004) is characterized by the values of $M = 0.5\,M_\odot$, log $g = 5.5$ and $T_{\rm eff} = 30\,000$ K. Furthermore, it has been assumed that the model, in its initial configuration at time $t = 1$ yr, is a standard "second generation" model à la Charpinet et al. (1997) in which diffusive equilibrium between gravitational settling and radiative levitation of iron has been reached. A stellar wind is then turned on at a rate of 6×10^{-15} $M_\odot$/yr. The key question is then to find out when the model looses its capacity to drive pulsation modes.

Figure 5 illustrates some of our results. It shows the evolving distribution of Fe in the envelope of our representative model. The initial equilibrium distribution at the beginning of the simulation is the curve labelled "0.00" and highlighted, in part, by the heavy curve. We recall here that diffusive equilibrium is reached at a given shell when the outward radiative acceleration on an element can be equated to the downward effective gravitational acceleration. Because the radiative acceleration depends on the abundance of the element in question, the condition of equilibrium implies an abundance at a given depth which depends on the local conditions. Hence, the equilibrium abundance of a radiatively levitating element is a function of depth.

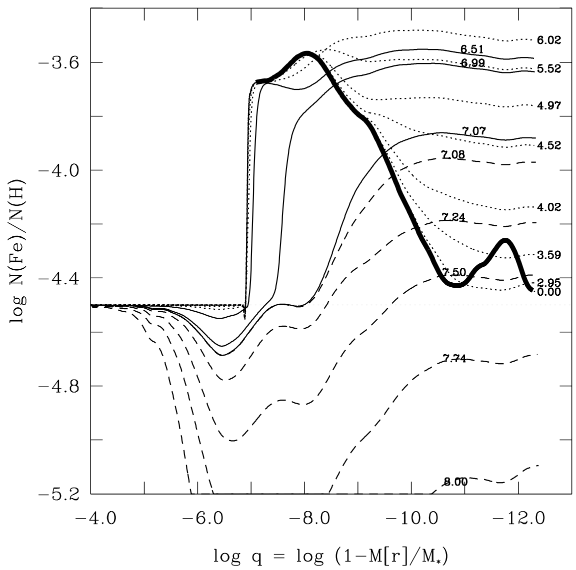

Fig. 5. Evolving distribution of iron in a representative sdB star model in the presence of a weak stellar wind. Only the envelope part of the stellar model is shown since the "action" is confined there. The heavy solid curve labelled "0.00" illustrates part of the initial distribution that is provided by the condition of diffusive equilibrium between gravitational settling and radiative levitation. Each curve is labelled by the logarithmic value of the time elapsed (in years) since the wind was turned on in the simulation. The dotted (solid) curves correspond to phases during which the Fe abundance in the driving region increases (decreases) while *p*-mode pulsations can be driven. The dashed curves, starting at an age of $10^{7.08}$ yrs, correspond to late phases when the Fe abundance in the driving region has dropped to values too small for pulsational driving to be possible.

As time goes by, the presence of a weak stellar wind progressively perturbs this equilibrium profile and, ultimately, the whole reservoir of levitating Fe is swept away. This is the case, for instance, for the profile labelled "8.00" that corresponds to the Fe distribution after 10^8 yrs of evolution. Thus, at the end of the simulation, the whole envelope becomes depleted of iron as compared to its normal value of $\log N(\mathrm{Fe})/N(\mathrm{He}) = -4.5$. On the other hand, there is an intermediate phase during which Fe pollution reaches its maximum across the outermost layers. This is shown by the profile obtained after $10^{6.02}$ yrs of evolution. After that phase, the abundance of Fe decreases monotonously throughout the envelope until the reservoir of levitating atoms is completely depleted.

In Fig. 5, the dotted and solid curves are associated with epochs when pulsational driving is possible. In fact, the model can drive a maximum number of modes precisely when Fe pollution is at a maximum in the driving region, i.e., after $10^{6.02}$ yrs of elapsed time in this particular simulation. After some $10^{7.08}$ yrs of evolution, however, the wind has done its damage and the model can no longer excite pulsation modes because the Fe abundance in the driving region has dipped below a critical level. The dashed curves thus correspond to epochs when the excitation of pulsation modes is no longer possible.

Fig. 5 also reveals the potential fate of the surface abundance of iron in a sdB star in the context of a wind scenario. According to our simulation, pulsators should show some Fe enhancements in their atmospheres – but note that this is a strong function of log g and $T_{\rm eff}$ – while nonpulsators may show enhanced, normal, or depleted abundances depending on their age and the wind's magnitude. This result has some important and unfortunate implications if the wind scenario that we have envisioned is realistic. Indeed, it may be difficult, if not impossible, to detect a spectroscopic signature that would discriminate between pulsating and nonpulsating sdB stars. This may be in line with the recent negative results reported from searches for a spectroscopic signature of pulsating sdB stars (e.g., Blanchette et al. (2006) and O'Toole et al., in preparation).

REFERENCES

Baran A., Pigulski A., Kogiel D., Ogloza W., Silvotti R., Zola S. 2005, MNRAS, 360, 737

Billères M., Fontaine G., Brassard P., Liebert J. 2002, ApJ, 578, 515

Billères M., Fontaine G., Brassard P., Charpinet S., Liebert J., Saffer R. A., Vauclair G. 1997, ApJ, 487, L81

Blanchette J.-P., Chayer P., Wesemael F. et al. 2006, Baltic Astronomy, 15, 301 (these proceedings)

Charpinet S. 1999, Ph.D. thesis, Université de Montréal

Charpinet S., Fontaine G., Brassard P. 2001, PASP, 113, 775

Charpinet S., Fontaine G., Brassard P., Chayer P., Rogers F. J., Iglesias C. A., Dorman B. 1997, ApJ, 483, L123

Charpinet S., Fontaine G., Brassard P. et al. 2006, Baltic Astronomy, 15, 305 (these proceedings)

Chayer P., Fontaine G., Fontaine M., Lamontagne R., Wesemael F., Dupuis J., Heber U., Napiwotzki R., Moehler S. 2004, Ap&SS, 291, 359

Fontaine G., Brassard P., Charpinet S., Green E. M., Chayer P., Billères M., Randall S. K. 2003, ApJ, 597, 518

Fontaine G., Green E. M., Brassard P., Charpinet S., Chayer P., Billères M., Randall S. K, Dorman B. 2004, Ap&SS, 291, 379

Green E. M., Fontaine G., Reed M. D., Callerame K., Seitenzahl I. R., White B. A., Hyde E. A., Østensen R., Cordes O., Brassard P., Falter S., Jeffery E. J., Dreizler S., Schuh S. L., Giovanni M., Edelmann H., Rigby J., Bronowska A. 2003, ApJ, 583, L31

Hubeny I., Lanz T. 1995, ApJ, 439, 875

Kilkenny D., Koen C., O'Donoghue D., Stobie R. S. 1997, MNRAS, 285, 640

Kilkenny D., O'Donoghue D., Reed M. D. et al. 2006, Baltic Astronomy, 15, 317 (these proceedings)

Lanz T., Hubeny Y. 1995, ApJ, 439, 905

Oreiro R., Pérez Hernández F., Ulla A., Garrido R., Østensen R., MacDonald J. 2005, A&A, 438, 257

Schuh S. L., Huber J., Green E. M., O'Toole S. J., Dreizler S., Heber U., Fontaine G. 2005, in 14th European Workshop on White Dwarfs, eds. D. Koester & S. Moehler, ASP Conf. Ser., 334, 530